Chemistry–A European Journal
Research Article
doi.org/10.1002/chem.202303250
Chemistry Europe
European Chemical Societies Publishing
www.chemeurj.org

Light-Induced Charge Separation in Covalently Linked BODIPY-Quinone-Alkyne Dyads

Sebastian Knoll,[a] Clara Zens,[b] Tamar Maisuradze,[b] Heiner Schmidt,[b, d] Stephan Kupfer,*[b] Linda Zedler,*[d] Benjamin Dietzek-Ivanšić,[b, d] and Carsten Streb*[a, c]

Visible light-induced charge separation and directional charge transfer are cornerstones for artificial photosynthesis and the generation of solar fuels. Here, we report synthetic access to a series of noble metal-free donor-acceptor dyads based on bodipy light-absorbers and redox-active quinone/anthraquinone charge storage sites. Peripheral functionalization of the quinone/anthraquinone units with alkynes primes the dyads for integration into a range of light-harvesting systems, *e.g.*, by Cu-catalyzed cycloadditions (CLICK chemistry) or Pd-catalyzed C–C cross-coupling reactions. Initial photophysical, electrochemical and theoretical analyses reveal the principal processes during the light-induced charge separation in the reported dyads.

Introduction

Natural and artificial photosynthetic schemes rely on the ability to combine visible light-driven charge separation with directional proton-coupled electron transfer.[1–3] In both systems, this ability forms the basis to access solar fuels by coupled (photo−)redox reactions such as water oxidation[4] and proton reduction.[5] Artificial systems often employ donor-acceptor dyads to study and realize (proton-coupled, multiple) electron transfer (PCET) processes.[6] Early pioneering dyads were often based on a noble metal complex photosensitizer linked to an organic charge storage site.[7,8] Often, these systems used ruthenium, iridium or osmium based photosensitizers[8] combined with redox-active charge storage sites ranging from organic redox-active molecules (e.g., quinone derivatives)[9] to fullerenes[10,11] and molecular metal oxides.[12,13] More recently, noble metal-free dyads based on earth-abundant components have been developed, leading to prototypes with increased technological importance. Prime examples utilize 3d metal complexes or organic dyes as light absorbers: for example, Kennis and co-workers developed Zinc-porphyrin light-absorbers covalently linked to carotenoid structures as models to rationalize energy transfer and dissipation in natural photosynthesis.[14] Wasielewski and co-workers used a Zn-containing chlorophyll derivative as light-absorber, linked to a perylene-acceptor to study quantum interference effects as a function of the covalent linkage between both components.[15]

Wenger and co-workers, provided a huge variety of ruthenium based dyads featuring different donor-acceptor frameworks, long range PCET dyads or even bodipy based platinum systems.[16–19] Purely organic dyads have been designed, e.g., by linking perylene dyes to triarylamines for use in dye-sensitized solar cells.[20] Also, bodipy dyes have been linked to quinones as a means of modulating fluorescence in the resulting dyads,[21] to efficiently generate charge separated states,[22] to drive electron storage in molecular metal oxides[23] or for the direct light-driven hydrogen evolution.[24] One current challenge in the field is the design of noble metal-free dyads which can subsequently be linked to other functional units, e.g., to catalysts for light-driven hydrogen evolution, CO_2 reduction or water oxidation. To this end, peripheral reactive sites, e.g., phenols, carboxylic acids,[25] alkynes, aromatic halides[26] and azides[27] have been incorporated into dyes and dyads to enable a broad scope of linkage chemistries, including ester/amide formation,[25,28] C–C-coupling reactions[29] as well as dipolar cycloadditions (including CLICK chemistry).[26,27]

Here, we report the design and synthesis of bodipy-quinone/anthraquinone donor-acceptor dyads using a facile CLICK chemistry approach.[6] The fundamental dyad properties were analyzed in a synergetic approach that combines synthesis, spectroscopy and theory. We demonstrate that understanding of the underlying photophysics as well as redox properties can be used to predict energy dissipation processes of the dyads upon visible light excitation. We also report the introduction of a peripheral alkynyl group on the quinone to facilitate subsequent coupling reactions such as CLICK chemistry or Pd-catalyzed cross-couplings to link the dyad to other functional units, including catalysts, polymers or surfaces.

[a] S. Knoll, Prof. Dr. C. Streb
Institute of Inorganic Chemistry I, Ulm University, Albert-Einstein-Allee 11, 89081 Ulm, Germany
[b] C. Zens, T. Maisuradze, H. Schmidt, Dr. S. Kupfer, Prof. Dr. B. Dietzek-Ivanšić
Institute of Physical Chemistry, Friedrich Schiller University Jena, Helmholtzweg 4, 07743 Jena, Germany
E-mail: stephan.kupfer@uni-jena.de
[c] Prof. Dr. C. Streb
Department of Chemistry, Johannes Gutenberg University Mainz, Duesbergweg 10–14, 55128 Mainz, Germany
E-mail: carsten.streb@uni-mainz.de
[d] H. Schmidt, Dr. L. Zedler, Prof. Dr. B. Dietzek-Ivanšić
Leibniz Institute of Photonic Technology, Albert-Einstein-Straße 9, 07745 Jena, Germany
E-mail: linda.zedler@leibniz-ipht.de

Supporting information for this article is available on the WWW under https://doi.org/10.1002/chem.202303250

Results and Discussion

Electron Bridge Synthesis

The quinone-based electron bridge was synthesized in six steps (see ESI, Figure S1), starting with the commercially available hydroquinone (1,4-dihydroxybenzene). First, the hydroxy group was protected by a slightly modified methylation procedure, using dimethyl carbonate (DMC) and 1,8-diazabicyclo(5.4.0)undec-7-ene (DBU) as catalyst, resulting in the isolation of 1,4-dimethoxybenzene.[30] Standard iodination with iodine monochloride for electron rich aromatics gave 1,4-diiodo-2,5-dimethoxybenzene. This was deprotected with boron tribromide and quenched with water to afford 2,5-diiodobenzene-1,4-diol. The trimethylsilyl (TMS)-protected acetylene moiety was introduced *via* a palladium/copper catalyzed sp–sp^2 C–C coupling reaction (Sonogashira–coupling); the resulting species was then protected by reaction with chloro(triisopropyl)silane in the presence of imidazole as catalyst, giving ((2,5-bis((triisopropylsilyl)oxy)-1,4-phenylene)bis(ethyne-2,1-diyl))bis-(trimethylsilane). TMS group cleavage was achieved using an alkaline methanolic potassium carbonate solution to give ((2,5-diethynyl-1,4-phenylene)bis(oxy))bis (triisopropylsilane) as the quinone-based protected electron bridge.[31–34] Full synthetic and analytical details are presented in the ESI.

The anthraquinone based electron bridge was synthesized in four steps (see ESI, Figure S2), starting from the commercially available 2,6-diaminoanthracene-9,10-dione. Reacting of this species with *tert*-butyl nitrite and copper(II) bromide gave the 2,6-dibromoanthracene-9,10-dione derivative. The subsequent palladium/copper catalyzed sp–sp^2 C–C coupling reaction with TMS-acetylene resulted in the formation of 2,6-bis ((trimethylsilyl)ethynyl)anthracene-9,10-dione.[35,36] For solubility reasons, the anthraquinone derivative was reduced and protected in a one-pot reaction using zinc powder as reducing agent and chloro(triisopropyl)silane as the reactant, yielding ((9,10-bis((triisopropylsilyl)oxy)anthracene-2,6-diyl)bis(ethyne-2,1-diyl)) bis(trimethylsilane). TMS-group cleavage was performed using a methanolic potassium carbonate solution, resulting in the anthraquinone-based protected electron bridge, ((2,6-diethynylanthracene-9,10-diyl)bis(oxy))bis(triisopropylsilane).

Bodipy Dyes

In contrast to the published synthesis route of fluorescent, azide functionalized bodipy dyes, starting from p-nitrobenzaldehyde towards the nitro functionalized bodipy dye with subsequent nitro group reduction and the follow up amine diazotation-substitution reaction,[37–39] our route reverses the azide introduction path and the bodipy condensation path. Therefore, a highly fluorescent bodipy dye was synthesized in three steps (see ESI, Figure S3), starting from commercial p-bromobenzyl alcohol. A copper(I) iodide – catalyzed nucleophilic aromatic substitution (*i.e.*, aromatic Finkelstein reaction), was used to give the p-azidobenzyl alcohol. Subsequent oxidation with manganese(IV)-oxide gave p-azido benzaldehyde. The bodipy dye was then synthesized by reacting the p-azido benzaldehyde with 2,4-dimethylpyrrole under acid catalysis, subsequent oxidation and complexation of boron trifluoride etherate under alkaline conditions, giving $Me_4BodipyN_3$. Oxidative iodination with elemental iodine and iodic acid[40] in ethanol/water was used to synthesize the bis-iodinated product featuring iodo-substituents in 2- and 6-position of the dye, giving $I_2Me_4BodipyN_3$ (see ESI Figure S4).

Dyads

Quinone based dyads were synthesized in three steps (see Figure 1), using microwave assisted copper catalyzed azide-alkyne cycloaddition (CuAAC). To prevent a multi-functionalization of the bis-alkyne ((2,5-diethynyl-1,4-phenylene)bis(oxy))bis (triisopropylsilane), an excess of the electron bridge was used. This excess can be separated by column chromatography and reused. Thus, iodinated ($I_2Me_4BodipyN_3$) or non-iodinated ($Me_4BodipyN_3$) azide functionalized bodipy dyes were reacted with the quinone based electron bridge and a copper(I) catalyst to obtain the protected X_2Me_4Bodipy-BQ(TIPS) dyad (Me_4Bodipy-BQ(TIPS) and I_2Me_4Bodipy-BQ(TIPS)). After deprotection with potassium fluoride, the reduced X_2Me_4Bodipy-BQH_2 dyads were isolated (Me_4Bodipy-BQH_2 and I_2Me_4Bodipy-BQH_2), and subsequent oxidation led to the final X_2Me_4Bodipy-BQ dyads (Me_4Bodipy-BQ and I_2Me_4Bodipy-BQ), see Figure 1/Figure S5.

A similar synthesis was used to access the anthraquinone derivative, obtaining Me_4Bodipy-AQ(TIPS). (note: the I_2Me_4Bodipy-AQ(TIPS) derivative was not isolated as a pure product). Using the properties of anthraquinone, deprotection and oxidation were performed in one step using molecular oxygen to oxidize the intermediate 9,10-anthracenediol, leading to the final anthraquinone based dyads X_2Me_4Bodipy-AQ (Me_4Bodipy-AQ and I_2Me_4Bodipy-AQ), see Figure 2/Figure S6.

Characterization

The identity and purity of the reported compounds was established using ^{1}H, ^{13}C and ^{19}F NMR spectroscopy. Bodipy dyes and dyads were additionally characterized by UV-Vis absorption and emission spectroscopy as well as electrochemistry (see ESI, Section Characterization). The presence or absence of azide groups was detected based on characteristic azide and triazole vibrational modes observed by ATR-FT-IR; this approach was used to identify the successful coupling during the CLICK reaction.

Electronic Structure of the Dyads

UV-Vis absorption and emission spectra of the bodipy dyads are shown in Figures 3 and 4. The non-iodinated bodipy dyads

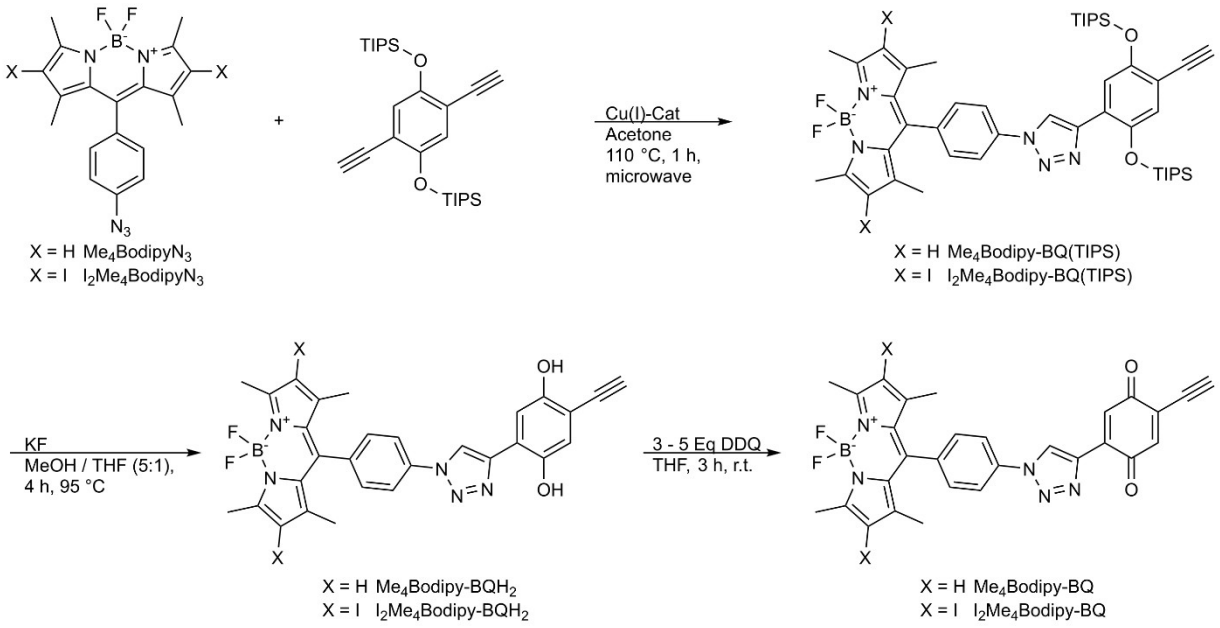

Figure 1. Synthesis scheme of X_2Me_4Bodipy-p-benzoquinone (X = H, I) based dyads.

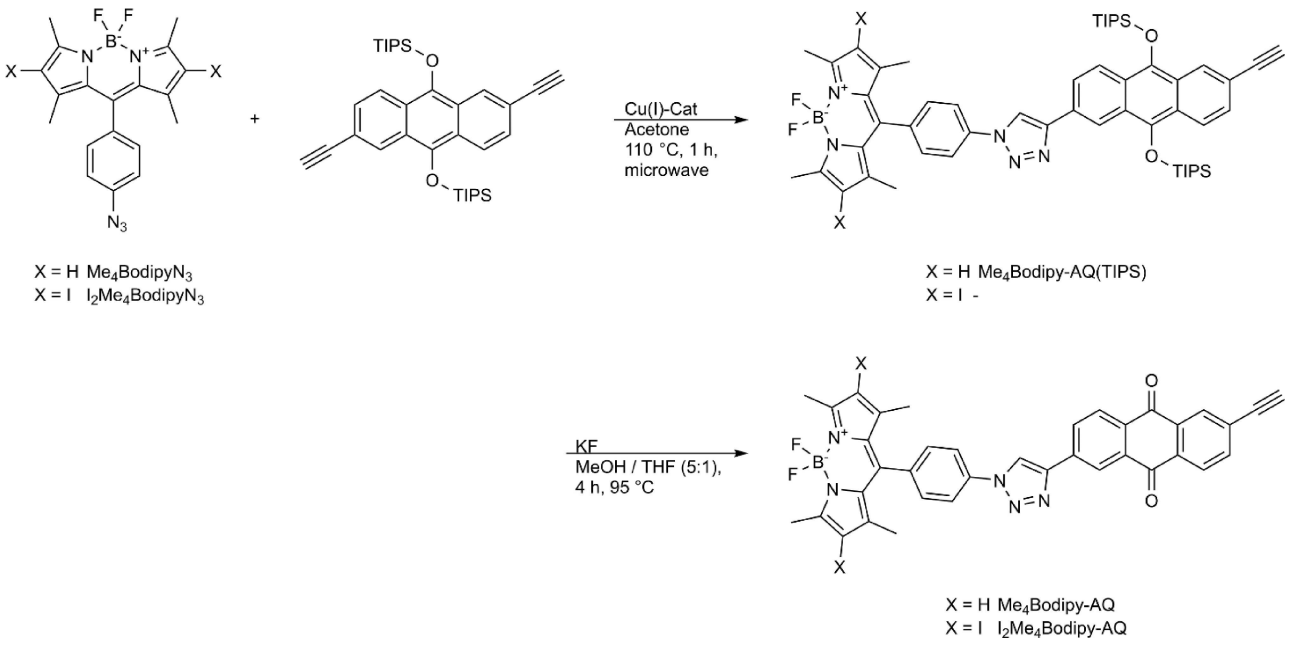

Figure 2. Synthesis scheme of X_2Me_4Bodipy-9,10-anthraquinone (X = H, I) based dyads.

feature high extinction coefficients (in $CHCl_3$ and MeCN) in the blue to green region between λ = 420 and 550 nm with maximum extinction coefficients ε_{max}~70,000 $L \cdot mol^{-1} \cdot cm^{-1}$ at λ_{max}~505 nm ($CHCl_3$) or λ_{max}~500 nm (MeCN) (Figure 3). The iodinated dyads show a bathochromic absorption shift to wavelengths of 450–580 nm. For the iodinated bodipys, similar absorption features are observed. Also, the lowest-energy transition is observed at ~533 nm (in MeCN) and ~540 nm (in $CHCl_3$) for iodinated bodipys (Figure 4).

Functionalization of the para–position of the phenyl ring does not affect the absorption wavelength. Figures 3 and 4 show computed vertical electronic absorption spectra overlayed with experimental UV-Vis data. To evaluate the electronic structure of the quinone-substituted bodipy dyads, quantum chemical simulations were performed at the DLNPO-NEVPT2 as well as at the density and time-dependent density functional (DFT and TDDFT) levels of theory. In contrast to DLPNO-NEVPT2 and in agreement with the literature,[41–48] the TDDFT calculated energies of the lowest dipole-allowed π→π* transition of the

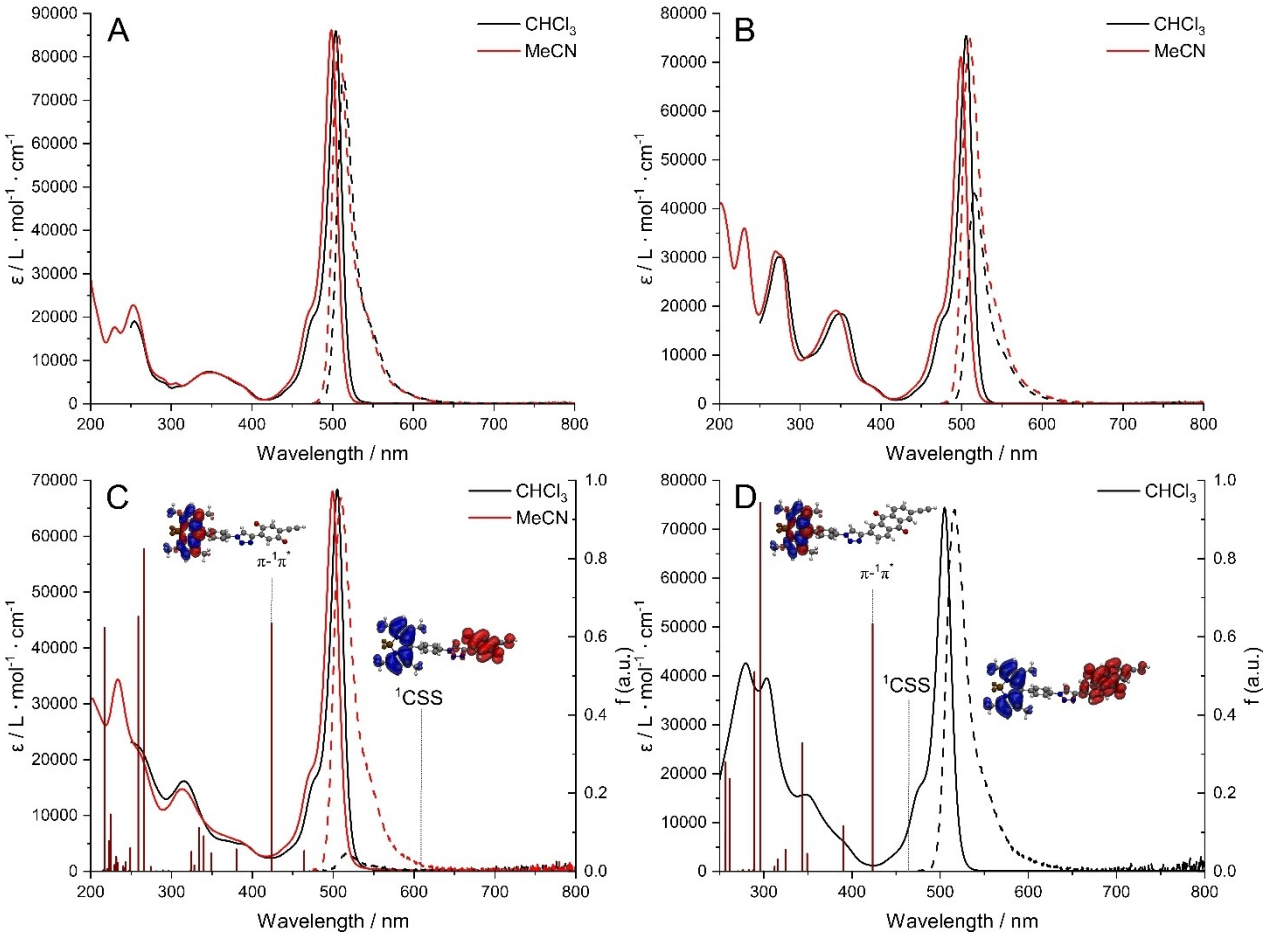

Figure 3. UV-Vis absorption spectra (solid lines, red and black), calculated vertical excitations (dark red) and normalized emission spectra (dashed lines) of A: Me_4Bodipy-N_3, B: Me_4Bodipy-BQH_2, C: Me_4Bodipy-BQ and D: Me_4Bodipy-AQ in $CHCl_3$ (black) and MeCN (red); $\lambda_{ex} = 470$ nm. Key electronic transitions as obtained at the TDDFT level of theory, namely the strongly dipole-allowed bodipy transition (π→π*) and excitation into the charge separated (CS) state, are labelled and indicated by charge density differences. Charge transfer takes place from red to blue.

bodipy chromophore are overestimated by approximately 0.3 eV (for further information, see SI). For Me_4Bodipy-BQ this excitation is (HOMO→LUMO + 1) predicted at 2.93 eV (423 nm). Upon iodine functionalization, i.e., for I_2Me_4Bodipy-BQ, this π→π* transition is shifted to 2.68 eV (463 nm). Note that for Me_4Bodipy-AQ and I_2Me_4Bodipy-AQ, identical excitation energies for the π→π* transition are calculated.

A noticeable difference between the species can be observed in the UV region between 250 and 400 nm. For $Me_4BodipyN_3$ and $I_2Me_4BodipyN_3$, these absorptions are related to π–π* transitions of substituted phenyl rings, while in the (anthra)quinone functionalized systems, these transitions are mostly related to π→π* transitions involving (anthra)quinone systems. Compared to reference spectra (see SI Figure S84) those absorption bands are shifted to lower energies due to the functionalization and the change in the (anthra)quinone symmetry. Three absorption bands at ~350 nm ($CHCl_3$)/346 nm (MeCN), 274 nm ($CHCl_3$ and MeCN) and 230 nm (MeCN) correspond mainly to transitions of the hydroquinone subunit, however, alkyne, phenyl as well as triazole moieties are involved as well. The benzoquinone subunits are mainly characterized via two absorptions in this region at ~312 ($CHCl_3$/MeCN) and ~260 nm ($CHCl_3$/MeCN). These absorption features correspond to calculated transitions in MeCN at 339 nm and 333 nm, 266 nm and 258 nm, as well as at 217 nm. The absorption features in the 330 nm region correspond to transitions from the π-orbital of the phenyl and the n-orbitals of the triazole to a π*-orbital of the quinone. The absorption feature centered at 260 nm originates from similar phenyl and quinone-related transitions. The absorption at 217 nm involves a transition from the π-orbitals of the bodipy chromophore and the alkyne-moiety towards the π*-system comprising the phenyl-, triazole and the quinone (Table S5). The anthraquinone functionalized bodipys were quantitatively measured only in $CHCl_3$ due to low solubility in MeCN. They show three absorption bands at ~350 nm, ~303 nm and ~279 nm. The calculated UV-Vis spectra in MeCN showed transitions at 343, 295 and 289 nm, as well as at 261 and 257 nm, respectively. The transition at 343 nm is a π→π* excitation of anthraquinone and involves π*-orbitals of alkyne moiety as well. States absorbing at 295 nm and 298 nm are transitions from π-orbitals of the phenyl triazole unit to π*-orbital of anthraquinone, with π→π* excitations within the anthraquinone moiety. Absorption at 261 nm involves π→π* orbitals of anthraquinone and π*-orbitals of alkyne group, while

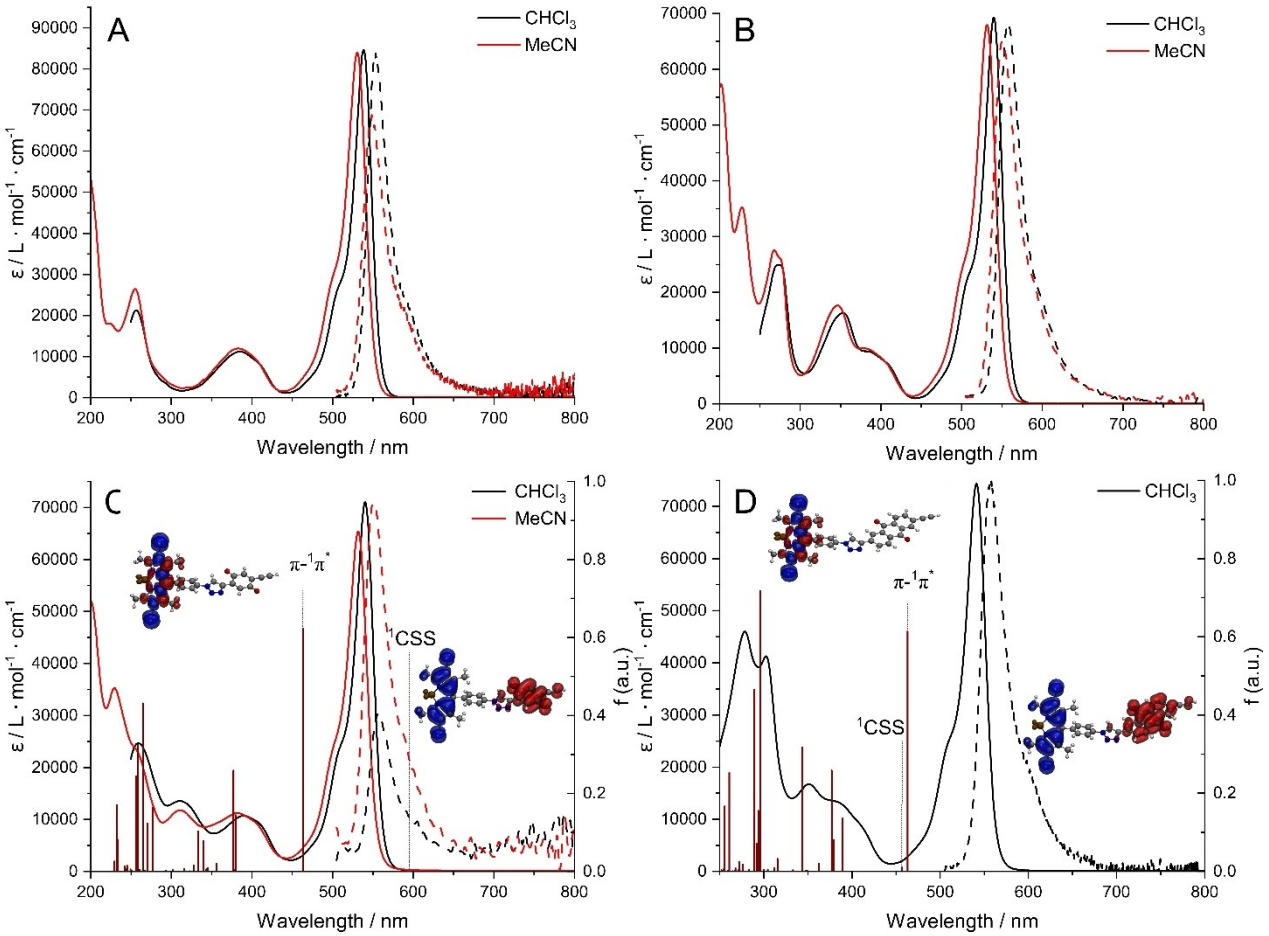

Figure 4. UV-Vis absorption spectra (solid lines, red and black), calculated vertical excitations (dark red) and normalized emission spectra (dashed lines) of A: I_2Me_4Bodipy-N_3 B: I_2Me_4Bodipy-BQH_2, C: I_2Me_4Bodipy-BQ and D: I_2Me_4Bodipy-AQ in $CHCl_3$ (black) and MeCN (red); $\lambda_{ex} = 500$ nm. Key electronic transitions as obtained at the TDDFT level of theory, namely the strongly dipole-allowed bodipy transition ($\pi \rightarrow \pi^*$) and excitation into the charge separated (CS) state, are labelled and indicated by charge density differences. Charge transfer takes place from red to blue.

states at 257 nm mainly involve transitions from π-orbitals of bodipy to π*-orbitals of anthraquinone (Table S6). In general, the non-iodinated bodipys provide a strong green fluorescence (except for Me_4Bodipy-BQ), when irradiated with blue light (470 nm, see Figure 5). This can be also observed in the emission spectra, where a strong asymmetric fluorescence band can be detected at ~514 nm ($CHCl_3$)/~510 nm (MeCN). After iodination in the bodipys' 2,2′ position, a diminished and bathochromic shifted emission signal can be observed at ~558 nm ($CHCl_3$)/552 nm (MeCN), due to the possible population of triplet excited states.[48] A drop of more than 90% in signal intensity is observed when comparing the non-iodinated species Me_4BodipyN_3 with the iodinated I_2Me_4BodipyN_3 (see SI Figure S81). Also, oxidation of Me_4Bodipy-BQH_2 to Me_4Bodipy-BQ resulted in a further drop of emission intensity (by ~90% in MeCN/~99% in $CHCl_3$). A similar, but less pronounced effect was observed for I_2Me_4Bodipy-BQH_2 and I_2Me4Bodipy-BQ (emission decrease ~66–73% in MeCN/~80–89% in $CHCl_3$) (see SI figures S82–83). Additionally, emission quantum yields have been determined. As expected, and in accordance with the featured emissions, a drop in the emission quantum yield could be observed after dyad iodination, as well as after the oxidation from the hydroquinone towards the quinone derivative. Therefore, quantum yields between 10% and 41% could be determined for Me_4Bodipy-BQH_2 ($CHCl_3$: 40.7%, MeCN: 36.7%) and Me_4Bodipy-AQ ($CHCl_3$: 12.7%, MeCN: 10.5%), while iodinated and oxidized dyads only feature quite low quantum yields between 0.5% and 4.5%; Me_4Bodipy-BQ ($CHCl_3$: 1.7%, MeCN: 3.1%), I_2Me_4Bodipy-BQH_2 ($CHCl_3$: 4.5%, MeCN: 2.3%), I_2Me_4Bodipy-BQ ($CHCl_3$: 0.7%, MeCN: 0.5%), I_2Me_4Bodipy-AQ ($CHCl_3$: 3.3, MeCN: 3.2%). Due to a decrease in electron density in the quinone subunit and the lower lying orbitals, a new radiationless deactivation pathway is accessible. We also note that the emission features show a weak solvatochromism. The Stokes shift of all compounds is between 47 meV (379 cm^{-1}) and 80 meV (645 cm^{-1}) and does not change significantly between different solvents. Slightly larger Stokes shifts are observed for the iodinated bodipys compared with the non-iodinated species. A small Stokes shift relates to a minor structural rearrangement within the excited state of the molecule.

Calculated emission data in MeCN, as obtained in the fully relaxed $\pi \rightarrow \pi^*$ equilibrium structure, show an emission energy of 2.77 eV (447 nm) for Me_4Bodipy-BQ, 2.53 eV (489 nm) for

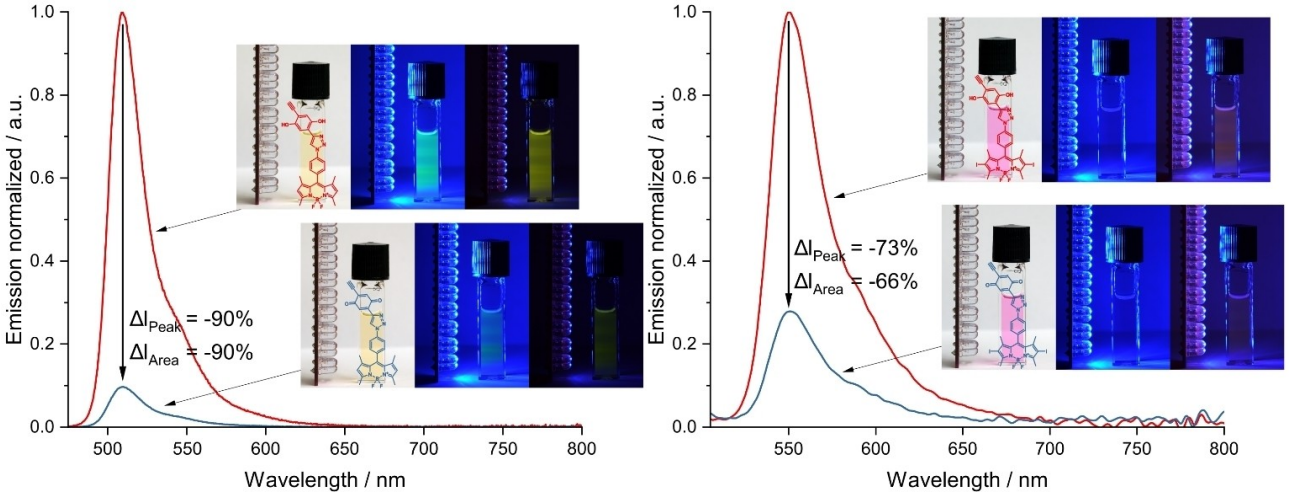

Figure 5. Left: Normalized emission spectra of Me_4Bodipy-BQH_2 (red line) and Me_4Bodipy-BQ (blue line) in MeCN (λ_{ex} = 470 nm). Inset: photographs of emission features: left: daylight without irradiation, middle: irradiation (470 nm); right: irradiation (470 nm) with blue light lens-filter. Right: Normalized emission spectra of I_2Me_4Bodipy-BQH_2 (red line) and I_2Me_4Bodipy-BQ (blue line) in MeCN (λ_{ex} = 500 nm, FFT filtered). Inset: photographs of emission features: left: daylight without irradiation (470 nm), middle: irradiation; right: irradiation (470 nm) with blue light lens-filter.

I_2Me_4Bodipy-BQ, 2.75 eV (451 nm) for Me_4Bodipy-AQ, and 2.53 eV (490 nm) for I_2Me_4Bodipy-AQ. As mentioned above, the simulated TDDFT energies of these π→π* transitions are systematically overestimated by ~0.3 eV. This is also the case for the emission, as the same underlying electronic transition is involved. The relaxation of the π→π* singlet excited state does not involve major structural changes compared to the ground state geometry. For Me_4Bodipy-BQ the calculated RMSD between the ground state and the relaxed π→π* singlet excited state is merely 0.42 Å. Hence, only small Stokes shifts are observed both in theory and experiment. The calculated Stokes shifts of 0.16 eV and 0.18 eV for the non-iodinated Me_4Bodipy-BQ and Me_4Bodipy-AQ, respectively, and to 0.15 eV in case of the corresponding iodinated species are in good agreement with the experimental observations. The overestimation of the TDDFT-predicted Stokes shifts is likely related to the slightly altered electronic character of the excited state upon equilibration, and thus, to the approximate treatment of electron correlation. In contrast, simulated Stokes shifts of the excited I_2Me_4Bodipy-BQ and I_2Me_4Bodipy-AQ are slightly underestimated. Likewise, we suspect this discrepancy to be mainly related to the applied non-equilibrated solvent model. Experimentally, the rather slow excited state equilibration is accompanied by a relaxation of the adjacent solvent shell, which is typically taken into account computationally by employing an equilibrium model of solvation in the frame of a polarizable continuum model. However, as equilibration of the continuum solvent model leads to implausible energies for the excited states (Figure S88 and Table S9), the respective equilibration was omitted. In consequence, the relative relaxation energies of the iodinated bodipy species are smaller than expected.

Low Temperature Emission Spectroscopy and Calculation of Gibbs Free Energy Using the Rehm Weller Method[49,50]

To gain a deeper insight into the system, and to assess whether electron transfer from bodipy-based excited states to the quinone is possible, low-temperature emission spectroscopy and electrochemical analyses were performed. Furthermore, quantum chemical simulations on I_2Me_4Bodipy-BQ, Me_4Bodipy-BQ, I_2Me_4Bodipy-AQ, and Me_4Bodipy-AQ were carried out to obtain mechanistic insight with respect to the accessible excited-state relaxation pathways. As shown in Figures 6 and 7, the chromophore emission wavelength is not influenced by the oxidation state of the electron bridge. Thus, low temperature (77 K) emission spectra for BQ species were performed using the BQH_2 species to gain higher-quality data. Compared to room temperature emission spectra, the emission band shape at 77 K is narrowed, and three vibrational features (at 509 nm, 545 nm and ~589 nm for Me_4Bodipy-BQH_2/AQ, at 547 nm, 589 nm and ~640 nm for I_2Me_4Bodipy-BQH_2/AQ) based on the same electronic state can be observed. This vibrational shift of *ca.* 1297 cm^{-1}, which can be assigned to the aromatic C–N stretching mode. This cluster of states can be considered as one state in thermal equilibrium.[51] For iodinated bodipy dyads, a weak triplet emission was observed also in the near infrared region. This signal was separated into two vibrational modes (763 nm and 795 nm) with a shift of 527 cm^{-1} (see Figure 7). Additionally, an anthraquinone triplet emission signal was raised for I_2Me_4Bodipy-AQ, lying between the two triplet bodipy emissions. Low temperature emission spectra were used to approximate the E_{00} transition of the bodipy subunit, thus, giving access to the energy of the photoexcited state. The energetics of the non-radiative process, i.e., the electron transfer from the excited donor subunit (bodipy) to the acceptor subunit (quinone), was analyzed based on electrochemical measurements (see Figures 6 and 7). To this end, the half-wave

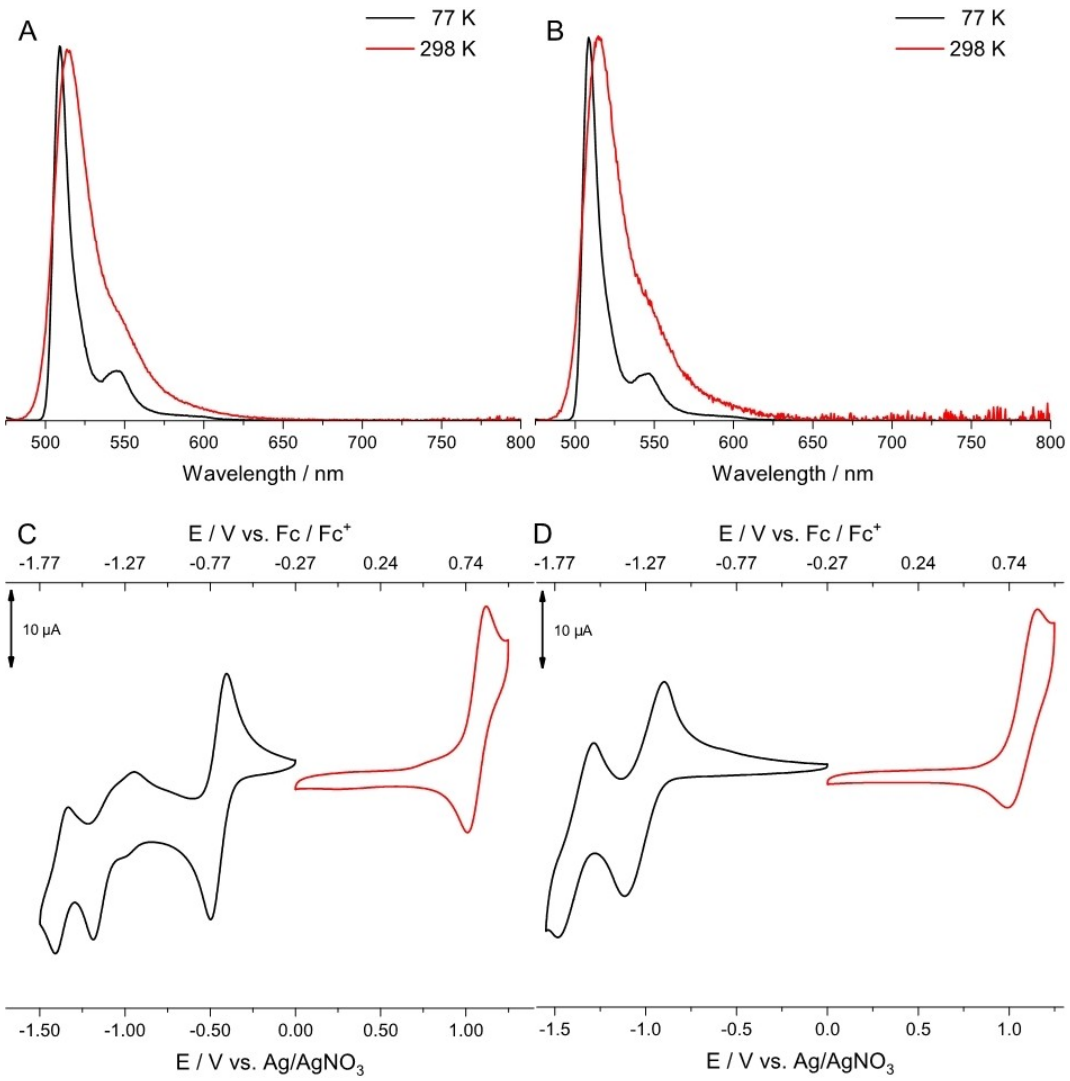

Figure 6. Emission spectra of (A) Me_4Bodipy-BQH_2; (B) Me_4Bodipy-AQ at 77 K (black) and 298 K (red) in a solvent matrix of 2.5 vol-% $CHCl_3$ and 97.5 vol-% ethanol:methanol (4:1, v:v): λ_{ex} = 470 nm. Cyclic voltammetry of (C) Me_4Bodipy-BQ; (D) Me4Bodipy-AQ reductive cycle (black) and oxidative cycle (red) in dry and degassed dichloromethane, using 0.1 M nBu$_4$NPF$_6$ as supporting electrolyte.

potential difference between the first oxidative redox process (bodipy/bodipy$^{+\bullet}$) and the first reductive redox process (quinone/quinone$^{-\bullet}$) was determined (E_{red}–E_{ox}), to obtain the electron transfer Gibbs energy ΔG_{ET}. In a first approximation, the difference of ΔG_{ET} and the E_{00} value are a measure of the driving force to populate the acceptor molecule after a photo-excitation process of the donor molecule (details of calculations and the Gibbs energy for photoinduced electron transfer can be found in the ESI).

This Rehm-Weller approximation shows that for the non–iodinated bodipy, containing the quinone subunit, a negative value in the range between $\Delta G_{PET,Onset}$(Me_4Bodipy-BQ) = −0.96 eV and $\Delta G_{PET,Maximum}$(Me_4Bodipy-BQ) = −0.92 eV is calculated. This suggests that an exergonic photoinduced electron transfer from the bodipy donor to the quinone acceptor is possible, see scheme in Figure 8. Similar data are calculated for the non–iodinated bodipy containing the anthraquinone subunit ($\Delta G_{PET,Onset}$(Me_4Bodipy-AQ) = −0.41 eV; $\Delta G_{PET,Maximum}$ (Me_4Bodipy-AQ) = −0.37 eV). A reduced driving force is expected, as the anthraquinone subunit features a higher-lying LUMO compared with the quinone species. The situation for the iodinated dyads is more complex, as the low-temperature spectroscopy had already indicated the population of singlet as well as triplet excited states. First we consider the singlet excitation, where the Rehm-Weller approximation still shows exergonic photoinduced electron transfer ($\Delta G_{PET,Onset}$ (I_2Me_4Bodipy-BQ) = −0.66 eV/$\Delta G_{PET,Maximum}$ (I_2Me_4Bodipy-BQ) = −0.61 eV, $\Delta G_{PET,Onset}$ (I_2Me_4Bodipy-AQ) = −0.13 eV/$\Delta G_{PET,Maximum}$ (I_2Me_4Bodipy-AQ) = −0.08 eV). The iodinated species therefore show lower driving forces compared with the non-iodinated species, which can be explained by the bathochromic emission shift, and thus a smaller HOMO-LUMO gap. Also, the iodinated bodipys show a more positive oxidation potential, and thus a lower-lying HOMO, due to the electron withdrawing effect of the iodine. These factors also affect the energy levels of the corresponding triplet state, where the ΔG^{T}_{PET} (= ΔG_{PET} triplet

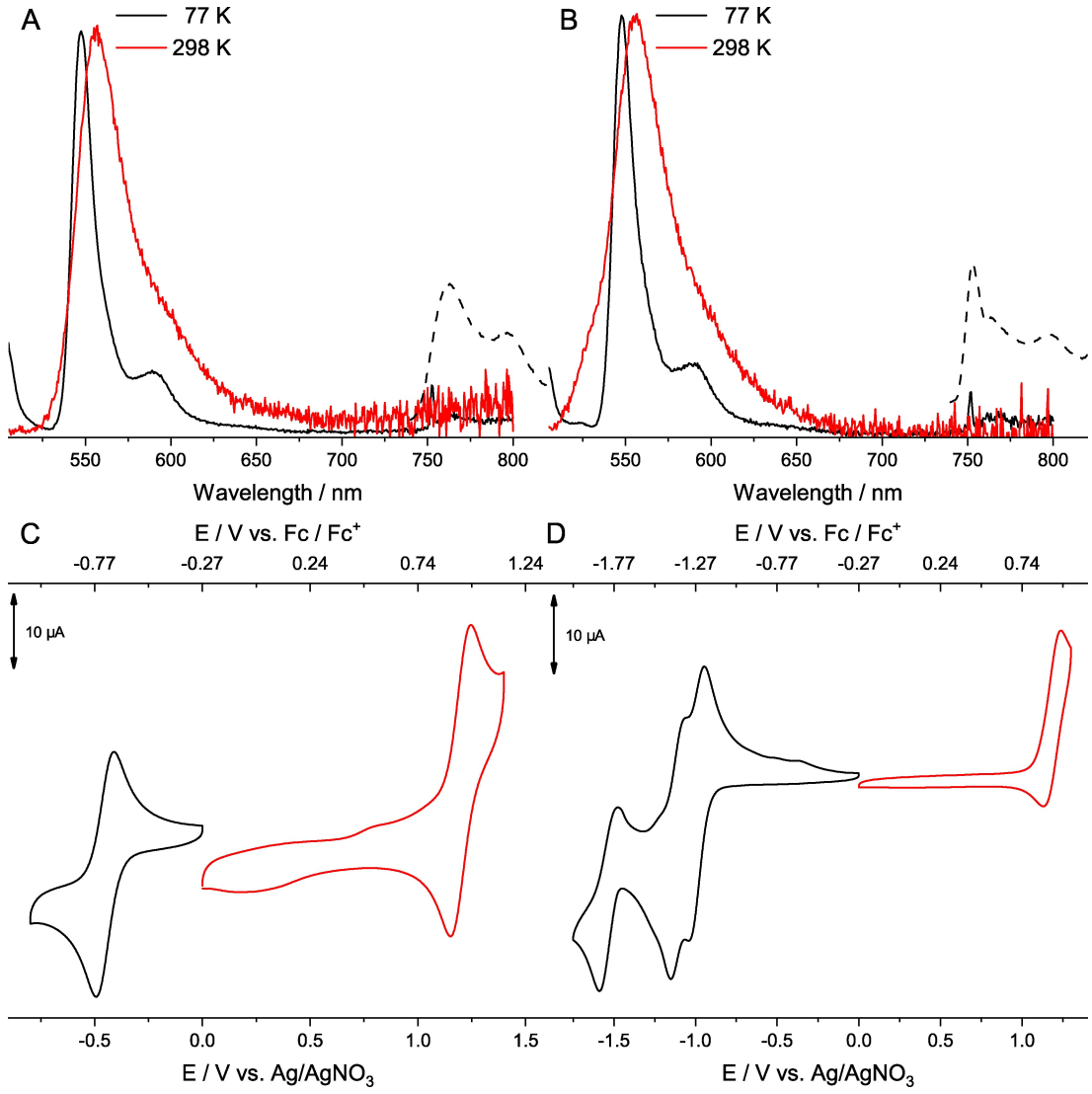

Figure 7. Emission spectra of 4 (A) I_2Me_4Bodipy-BQH_2 and (B) I_2Me_4Bodipy-AQ at 77 K (black, solid: singlet, dashed: triplet) and 298 K (red) in a solvent matrix of 2.5 vol-% $CHCl_3$ and 97.5 vol-% ethanol:methanol (4:1, v:v): $\lambda_{ex} = 500$ nm. Cyclic voltammetry of (C) I_2Me_4Bodipy-BQ; (D) I_2Me_4Bodipy-AQ reductive cycle (black) and oxidative cycle (red) in dry and degassed dichloromethane, using 0.1 M nBu$_4$NPF$_6$ as supporting electrolyte.

state) values are located near 0 eV for the benzoquinone-containing dyad, while for the anthraquinone derivative, positive ΔG^T_{PET} values are observed ($\Delta G^T_{PET,Onset}$(I_2Me_4Bodipy-BQ) = −0.02 eV/$\Delta G^T_{PET,Maximum}$ (I_2Me_4Bodipy-BQ) = 0.03 eV, $\Delta G^T_{PET,Onset}$(I_2Me_4Bodipy-AQ) = 0.51 eV/$\Delta G^T_{PET,Maximum}$(I_2Me_4Bodipy-AQ) = 0.56 eV). This indicates that there is no driving force for photoinduced electron transfer from the triplet excited states, as the donor triplet LUMO energy level is lower than the acceptor LUMO energy level.

Quantum chemical calculations at the TDDFT level of theory were carried out to address the energy levels of the key electronic states, *e.g.*, of the lowest energy π→π* state of the bodipy dyes as well as of the lowest energy CS state (bodipy→quinone) within the singlet and the triplet manifold. The driving force for the photoredox process of interest (ΔG_{PET}) was obtained based on the bodipy-centered π→π* state within its fully relaxed equilibrium and the relaxed CS state; see supporting information for details. Thereby, a driving force of −1.13 eV was obtained for Me_4Bodipy-BQ within the singlet manifold. In the case of I_2Me_4Bodipy-BQ a slightly smaller driving force of −0.81 eV is calculated (Table S3 and Figures S86/S87). These values correspond very well to the respective experimental values of −0.96 and −0.66 eV, respectively. The smaller driving force of the iodinated species is mainly caused by an energetically lowered singlet π→π* excited state (π→^{1}π*), while the energy of the singlet charge separated state (^{1}CSS) is almost unchanged for the iodinated and non-iodinated species. In the anthraquinone bodipy species compared to the benzoquinone bodipy species the π→^{1}π* state is almost not changed in energy. However, ^{1}CSS is increased in energy by about 0.7 eV depending on the respective geometry.

Hence, in case of Me_4Bodipy-AQ and I_2Me_4Bodipy-AQ much smaller ΔG_{PET} values of −0.43 eV and −0.11 eV were predicted, respectively. For I_2Me_4Bodipy-BQ, the triplet charge separated

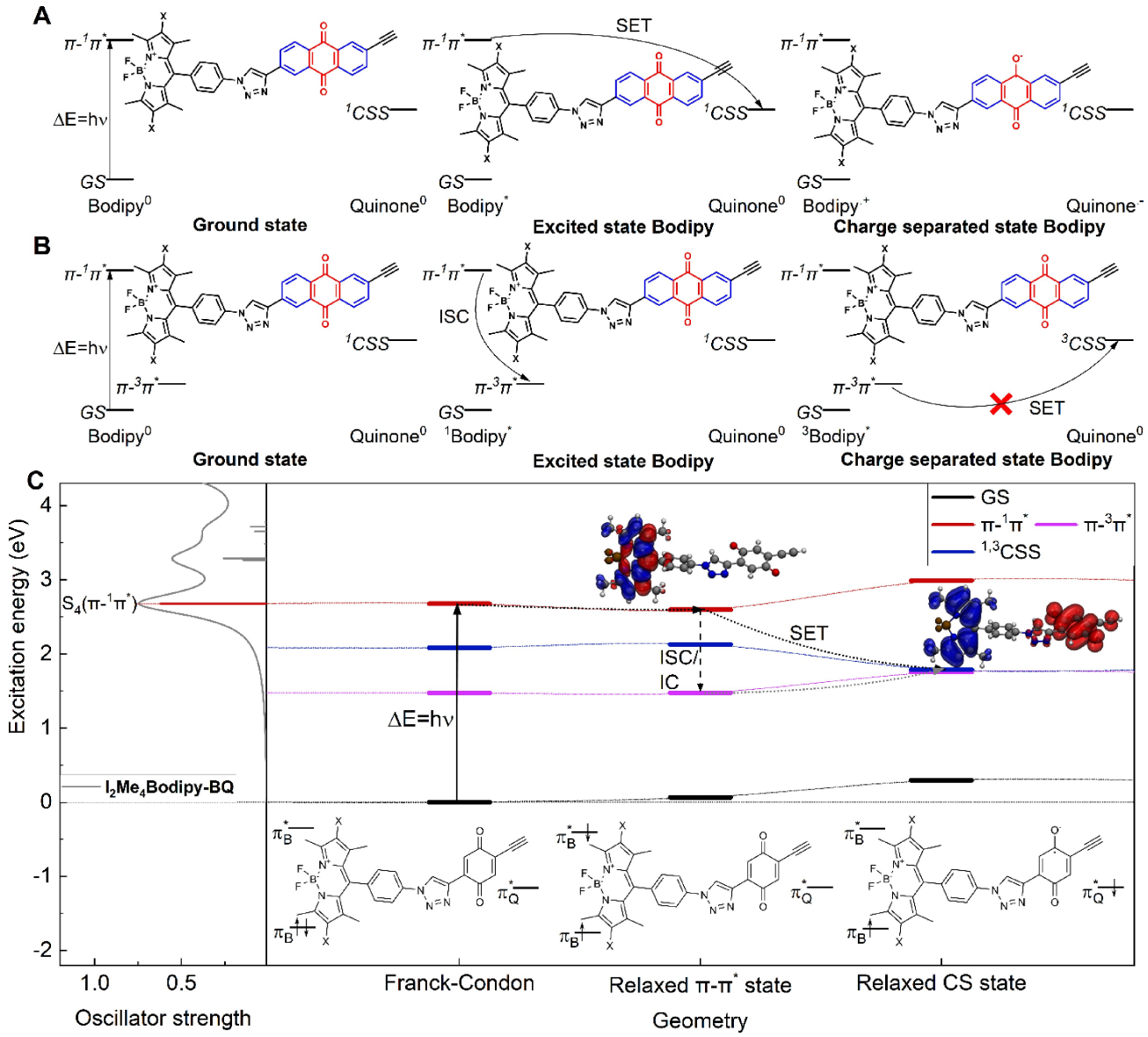

Figure 8. Process of the photoredox reaction shown using I_2Me_4Bodipy-BQ as an example. The ground state bodipy^0 is excited into the singlet π→π* state. From the relaxed singlet π→π* state the ^{1}bodipy* can either undergo a single electron transfer (SET) into the singlet charge separated state (^{1}CSS) (A) or an intersystem crossing into the triplet π→π* state. If the ^{1}Bodipy* underwent an intersystem crossing to the triplet π→π* state, the path of the SET is no longer available due to the higher energy of the triplet charge separated state.

state (^{3}CSS) is degenerate to the respective ^{1}CSS. This is a consequence of the large spatial distance between the unpaired electrons, i.e., leading to an exchange integral of ~0. However, in case of the locally excited π→π* state of the chromophore unit, the π→^{3}π* is lower than the π→^{1}π* by 1.21 eV in the Franck-Condon region. Here, the π→^{3}π* is 0.66 eV lower than the ^{3}CSS. This trend of reversed order in energy for the triplet state is seen in all optimized geometries within I_2Me_4Bodipy-BQ. Hence, the driving force for the electron transfer from the π→π* to the CS state is positive for the triplet states. For I_2Me_4Bodipy-AQ, ^{1}CSS is degenerate to the respective triplet state. π→^{3}π* is lower in energy by 1.27 eV compared to respective singlet state in the Frank-Condon region. Similar to I_2Me_4Bodipy-BQ, the π→^{3}π* states in all optimized geometries are lower in energy than the respective ^{3}CSS, therefore, the driving force for electron transfer from π→^{3}π* to ^{3}CSS is positive for I_2Me_4Bodipy-AQ as well (see Figure S87).

From an experimental point of view, the singlet emission spectra show a drop in intensity going from the reduced hydroquinone subunit to the oxidized benzoquinone containing dyad (see Figure 5), indicating the access to a non-emissive deactivation process, possibly taking place via an electron transfer from the excited donor molecule (Me_4Bodipy/I_2Me_4Bodipy) to the acceptor molecule (benzoquinone). In synergy, Gibbs free energy calculations based on the Rehm-Weller approximation and the quantum chemical simulations on the involved photoredox intermediates, suggest that this process is exergonic for singlet excited donor molecules

(Me_4Bodipy/I_2Me_4Bodipy) but endergonic for triplet excited donor molecules (I_2Me_4Bodipy).[52] These findings can be summarized as shown in Figure 8B where electron transfer *via* a singlet excited state is proposed. Figure 8A shows the scheme for the electron transfer via a singlet excitation followed by an inter-system crossing (ISC) into a triplet excited state without an electron transfer to the acceptor molecule.

Characterization of the Photoinduced Ultrafast Reactivity

In order to decipher the photoinduced ultrafast reactivity in the donor-acceptor dyads, femtosecond transient absorption spectroscopy was complemented by UV-vis spectro-electrochemistry. Transient absorption spectra of the donor-acceptor dyads Me_4Bodipy-BQ, I_2Me_4Bodipy-BQ, Me_4Bodipy-AQ and I_2Me_4Bodipy-AQ were recorded upon excitation at 500 nm, *i.e.*, within the bodipy-centered $\pi \rightarrow {}^1\pi^*$ absorption.[12,47] UV-Vis spectro-electrochemical measurements form the basis for simulating the spectral signatures of the intramolecular charge transfer states,[53,54] which is formed upon reduction of the quinone part and simultaneous oxidation of the bodipy unit (shown as dotted lines in the Figure 9).

The transient absorption spectra of the dyads Me_4Bodipy-BQ, I_2Me_4Bodipy-BQ, Me_4Bodipy-AQ and I_2Me_4Bodipy-AQ at various time delays after excitation consistently show an excited state absorption (ESA) at 350 nm, which is attributed to the $\pi \rightarrow \pi^*$-singlet state of the bodipy dye (Figure 9).[47] Based on literature, the ESA band at 450 nm as well as the broad ESA between 550 and 700 nm observed for the iodinated dyads are assigned to the bodipy triplet state.[47,55] The spectrally broad ground state bleach (GSB) between 460 and 620 nm at short delay times is consistent with the depletion of the bodipy ground state and is superimposed by a red shifted stimulated emission (SE). For Me_4Bodipy-AQ a GSB at around 400 nm is observed, which spectrally evolves to a band centered at 420 nm within 100 ps before it decays on a 1000 ps time scale. The 420 nm band correlates to the spectral signature of the reduced anthraquinone ligand and is therefore attributed to the light-induced formation of a CSS of unspecified multiplicity. According to UV-Vis spectro-electrochemical data, a positive differential absorption feature between 550 and 650 nm should

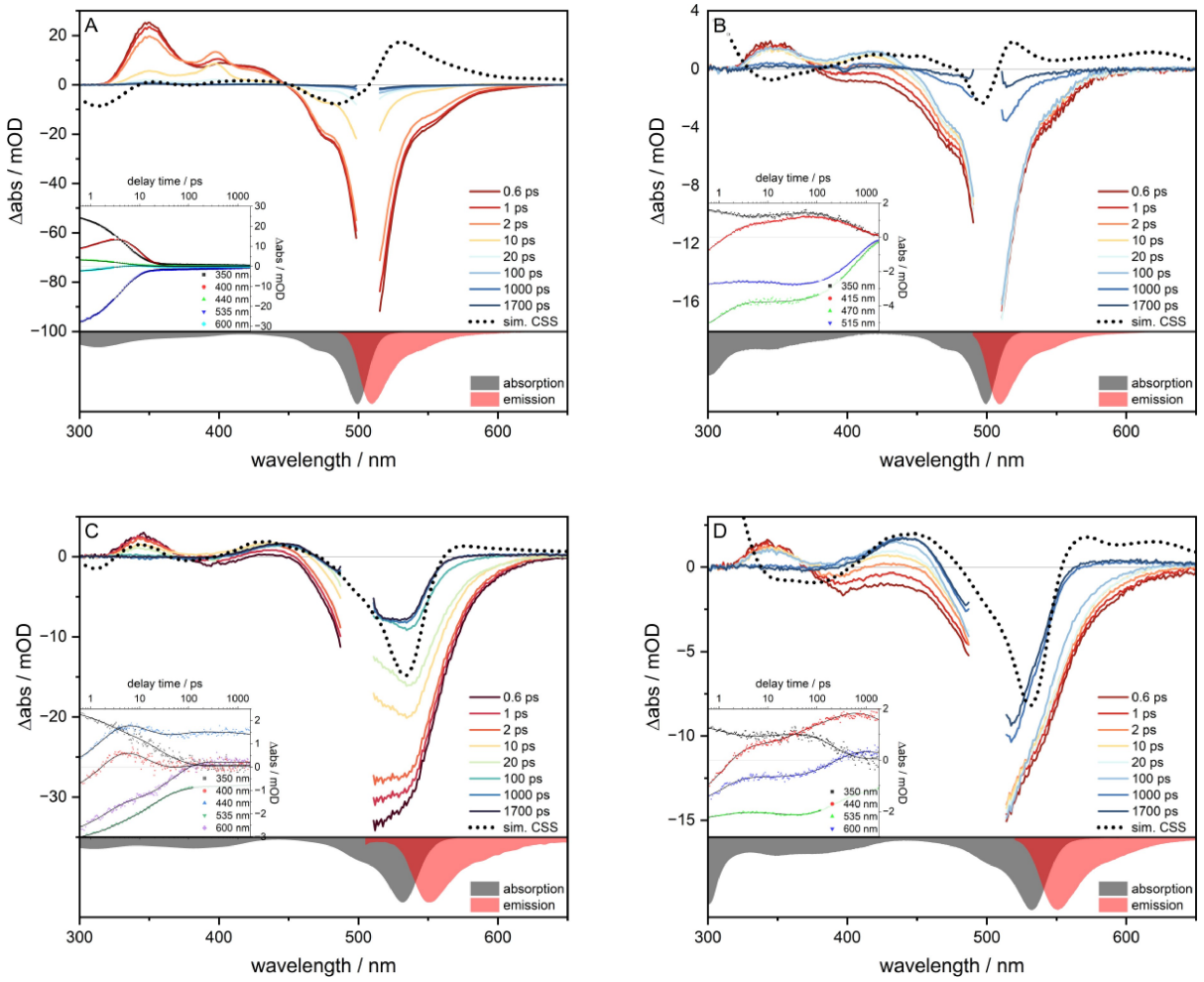

Figure 9. Femtosecond transient absorption spectra of (A) Me_4Bodipy-BQ, (B) Me_4Bodipy-AQ, (C) I_2Me_4Bodipy-BQ, (D) I_2Me_4Bodipy-AQ at certain delay times collected upon pumping at 500 nm in aerated MeCN. For comparison spectra obtained from UV-Vis spectro-electrochemical experiments (dotted lines) and the inverted and scaled steady state and emission spectrum were added (subsets). Insets: kinetic traces at specific wavelength (dots) and their fit traces (black lines), GSB traces for A (515 nm), B and D (535 nm) were divided by a factor of 5 and C (535 nm) by 10 for visibility.

be associated with the CSS. This signature has only low intensity in the TA spectra, as it spectrally overlaps with GSB and SE. For I_2Me_4Bodipy-AQ and I_2Me_4Bodipy-BQ the formation of a long-lived triplet state is observed at 430 nm,[47] which spectrally overlaps with the absorption of the simulated CSS at 450 nm (Figure 9).

Transient absorption spectra were fitted using the software package KiMoPack.[56] We applied either a three-component model (Me_4Bodipy-AQ, Me_4Bodipy-BQ) or a four-component model (I_2Me_4Bodipy-AQ, I_2Me_4Bodipy-BQ). Decay associated spectra (DAS, supporting information S89) reflect upon different kinetic processes, which were assigned by correlating the spectral features associated with the decay processes to simulated CSS spectra from UV-Vis spectroelectrochemistry. This procedure considers characteristic spectral features of different molecular species involved in the excited-state relaxation, e.g., bodipy-$\pi\rightarrow{}^3\pi^*$ or the ESA of reduced quinones at 440–450 nm and above 500 nm.[47,55,57–59]

We will start the discussion with Me_4Bodipy-BQ, in which optical excitation populates a bodipy-centered $\pi\rightarrow\pi^*$-transition (see Fig. S89A, S90A). Optical excitation of the bodipy fragment is followed by a fast process with a characteristic time constant of $\tau_1 = 3.5$ ps, which we assign to an intramolecular charge transfer (CT). This fast process populates a CSS, as inferred from the similarities of the DAS features and the inverted simulated CSS spectrum, e.g., a negative feature at 400 nm and a positive feature of the GSB. This initially populated charge separated state is referred to as CSS_1 and decays with a time constant of $\tau_2 = 5.8$ ps. DAS(τ_2) reflects the decay of the characteristic simulated CSS absorption at 400 nm and a decay of the GSB, which accounts for most of the decay to the ground state. A long-lived minor kinetic component associated with $\tau_3 > 2$ ns ("infinite") features spectral characteristics of a CSS decay as seen by positive absorption bands at 350 and 425 nm, which are also present in the simulated CSS and is thus far labelled as CSS_2.

Introduction of the iodine in I_2Me_4Bodipy-BQ (see Fig. S89C, S90C) modifies the excited-state relaxation process and two different decay channels are observed. In the first decay channel, a fast CT to a CSS (bodipy$^+$-BQ$^-$) with a time constant of $\tau_1 = 1.8$ ps occurs. The DAS of the respective component shows a positive spectral feature at 350 nm pointing to the depletion of the bodipy $\pi\rightarrow{}^1\pi^*$ state and negative features beyond 400 nm indicating the build-up of the CSS features at 440 nm. The increase in the differential absorption signal at 550 nm is likely associated with a broader excited-state absorption overriding the ground state bleach signal. Similar fast oxidative quenching of a photoexcited bodipy fragment has been reported in literature for bodipy-C_{60}-donor/acceptor-dyads, in which intramolecular CT was reported to take place on a sub-1-ps timescale.[60] We hypothesize that the resultant CSS relaxes by a spin-orbit coupled charge transfer (SOC-CT) into a bodipy-centered $\pi\rightarrow{}^3\pi^*$ state with a time constant of $\tau_2 = 14.6$ ps. DAS(τ_2) reflects the decay of the spectral features associated with the simulated CSS, i.e., a positive signal at 430 nm, while the negative signal above 500 nm can be understood as the build-up of a bodipy-centered triplet state.[47,55,57] Triplet state transitions are only possible for iodinated species according to calculations (see above). We assign the time constant of $\tau_3 = 49$ ps to vibrational relaxation followed by a CT to the CSS from the excited state S_1 in the second decay channel. A depletion of the excited bodipy* at 350 nm, a gain of simulated CSS signal at 440 nm and a loss of SE at 550 nm indicates this process starts from the relaxed $\pi\rightarrow{}^1\pi^*$ and leads to a CSS. Finally, the ground state is repopulated on a time scale greater than 2 ns, which represents the limit of experimentally accessible delay times. Consequently, the infinite component ($\tau_4 > 2$ ns) includes spectral features of both $\pi\rightarrow{}^3\pi^*$-bodipy species[47,57–59] and the CSS, both having ESA at 440–450 nm and above 500 nm as discussed earlier, and is therefore assigned to a decay of those two states back to the ground state.These long living bodipy triplet states are supported by literature.[47,55,57–59]

Me_4Bodipy-AQ (Figure S89B, S90B) forms a CSS within $\tau_1 = 1.1$ ps after optical excitation from the Franck-Condon region. This fast component is spectrally identical to the fastest component of I_2Me_4Bodipy-BQ (see previous paragraph). Therefore, we assign it to a similar CT process. However, also the process associated with the characteristic decay time $\tau_2 = 29$ ps shows spectral features associated with the formation of a CSS, i.e., a rise at 430 nm and an increase of the $\pi\rightarrow{}^1\pi^*$ bleach at 500 nm. We thus associate τ_2 with intramolecular CT from the thermally relaxed bodipy excited state. Finally, in Me_4Bodipy-AQ the CSS decays with a time constant of 635 ps back to the ground state, as supported by depletion of the CSS signal at 440 nm and depletion of the $\pi\rightarrow{}^1\pi^*$ bleach at 500 nm.

Comparing I_2Me_4Bodipy-AQ (Figure S89D, S90 D) with Me_4Bodipy-AQ (see previous paragraph) two spectrally similar fast decay components for I_2Me_4Bodipy-AQ with lifetimes of $\tau_1 = 1.2$ ps and $\tau_2 = 28$ ps are observed, which corresponds to a direct CT to the CSS within 1.2 ps or after vibrational cooling, i.e., from the vibrationally relaxed bodipy* state, within 28 ps. Comparison with UV-Vis-SEC data supports this assignment. i.e., the formation of a CSS directly from the hot excited $\pi\rightarrow{}^1\pi^*$ within 1.2 ps. The third component with $\tau_3 = 219$ ps features depletion of $\pi\rightarrow{}^1\pi^*$ at 350 nm and depletion of SE at 550 nm, meaning the process is starting out of the vibrational relaxed $\pi\rightarrow{}^1\pi^*$, and buildup of a signal at 450 nm typical for bodipy-$\pi\rightarrow{}^3\pi^*$ states.[47,57–59] Therefore this process is assigned to ISC to a bodipy triplet state. Analogous to I_2Me_4Bodipy-BQ the long-lived component ($\tau_1 > 2$ ns) is assigned to the decay of the bodipy-$\pi\rightarrow{}^3\pi^*$ and the CSS.

Figure S90 shows Jablonski diagrams reflecting the excited-state relaxation pathways discussed before. As known from literature CLICK-type triazoles can obstruct charge transfer between donor and acceptor moieties in dyad systems.[6] However, our results clearly show that fast forward charge transfer from the bodipy donor to the quinone acceptor via the triazole linker is possible.

Conclusions

In summary, we could present a synthetic approach to a series of bodipy-quinone dyads for light-induced charge separation. Experimental steady-state emission spectroscopy shows tremendous losses in emission intensity for the bodipy dye going from hydroquinone- to the benzoquinone-dyad indicating a charge transfer, which was confirmed by femtosecond transient absorption spectroscopy, spectro-electrochemical measurements, and quantum chemical simulations. Electrochemical measurements, combined with low-temperature steady-state emission spectroscopy gave access to Gibbs free energy of the photoinduced electron transfer. Quantum chemical calculations have been carried out to further elucidate the Franck-Condon photophysics as well as the emission and excited state electron transfer channels for the given set of molecular dyads. Thus, we could show, that a bodipy $\pi \rightarrow \pi^*$ excitation (with and without iodine substitution) leads to a charge separated state via electron transfer from the bodipy donor to a quinone acceptor. In addition, these simulations revealed that for the iodine-substituted bodipy dyes, the populated triplet states do not promote such an electron transfer, due to the unfavorable driving force ($\Delta G_{PET} \geq 0$). However, population of the charge-separated state is possible in the singlet manifold (prior to ISC). In a synergic fashion, this finding is based on quantum chemical calculations, the experimental determination of Gibbs free energy for the photoinduced electron transfer as well as on femtosecond transient absorption spectroscopy. With the help of femtosecond transient absorption spectroscopy, we could additionally provide first mechanistic insights on the population of charge separated states as well as the dynamics between singlet and triplet excited states within a long timeframe. Results gained from these measurements also showed, that a charge separated state is unlikely to be populated by a triplet excited state. We could also show, that a fast forward electron transfer in systems featuring a triazole linker is possible, even if described unfavored by literature.[6] Thus, future works can still utilize CLICK-chemistry based dyads for forward electron transfer.

Experimental Section

Full analytical, spectroscopic, theoretical, and crystallographic details are given in the Supporting Information.

Acknowledgements

The authors gratefully acknowledge the Deutsche Forschungsgemeinschaft DFG for financial support (projects TRR 234 "CataLight", projects A1, A4, project no: 364549901; SPP2102, "Light-controlled reactivity of metal complexes", project no: 359737763, 494988281). S.K. gratefully acknowledges a LGFG PhD fellowship by the State of Baden-Württemberg. C.S. gratefully acknowledges support by the JGU Mainz via the Gutenberg Research College and the Top-Level Research Area SusInnoScience. Open Access funding enabled and organized by Projekt DEAL.

Conflict of Interests

The authors declare no conflict of interest.

Data Availability Statement

The data that support the findings of this study are openly available in zenodo.org at 10.5281/zenodo.8406484, reference number 8406484.

Keywords: Bodipy · Dyads · Charge-Accumulation · Photosensitizer · Quinone

[1] S. Berardi, S. Drouet, L. Francàs, C. Gimbert-Suriñach, M. Guttentag, C. Richmond, T. Stoll, A. Llobet, *Chem. Soc. Rev.* **2014**, *43*, 7501–7519.
[2] I. McConnell, G. Li, G. W. Brudvig, *Chem. Biol.* **2010**, *17*, 434–447.
[3] T. Keijer, T. Bouwens, J. Hessels, J. N. H. Reek, *Chem. Sci.* **2021**, *12*, 50–70.
[4] R. Matheu, P. Garrido-Barros, M. Gil-Sepulcre, M. Z. Ertem, X. Sala, C. Gimbert-Suriñach, A. Llobet, *Nat. Chem. Rev.* **2019**, *3*, 331–341.
[5] V. Artero, M. Chavarot-Kerlidou, M. Fontecave, *Angew. Chem. Int. Ed.* **2011**, *50*, 7238–7266.
[6] C. Müller, S. Bold, M. Chavarot-Kerlidou, B. Dietzek-Ivanšić, *Coord. Chem. Rev.* **2022**, *472*, 214764.
[7] P. Laine, S. Campagna, F. Loiseau, *Coord. Chem. Rev.* **2008**, *252*, 2552–2571.
[8] O. S. Wenger, *Coord. Chem. Rev.* **2015**, *282–283*, 150–158.
[9] J. Hankache, M. Niemi, H. Lemmetyinen, O. S. Wenger, *Inorg. Chem.* **2012**, *51*, 6333–6344.
[10] M. S. Rodríguez-Morgade, M. E. Plonska-Brzezinska, A. J. Athans, E. Carbonell, G. de Miguel, D. M. Guldi, L. Echegoyen, T. Torres, *J. Am. Chem. Soc.* **2009**, *131*, 10484–10496.
[11] A. Polese, S. Mondini, A. Bianco, C. Toniolo, G. Scorrano, D. M. Guldi, M. Maggini, *J. Am. Chem. Soc.* **1999**, *121*, 3446–3452.
[12] F. A. Black, A. Jacquart, G. Toupalas, S. Alves, A. Proust, I. P. Clark, E. A. Gibson, G. Izzet, *Chem. Sci.* **2018**, *9*, 5578–5584.
[13] S. Amthor, S. Knoll, M. Heiland, L. Zedler, C. Li, D. Nauroozi, W. Tobaschus, A. K. Mengele, M. Anjass, U. S. Schubert, et al., *Nat. Chem.* **2022**, *14*, 321–327.
[14] R. Berera, C. Herrero, I. H. M. van Stokkum, M. Vengris, G. Kodis, R. E. Palacios, H. van Amerongen, R. van Grondelle, D. Gust, T. A. Moore, et al., *Proc. Nat. Acad. Sci.* **2006**, *103*, 5343–5348.
[15] G. Huang, M. A. Harris, M. D. Krzyaniak, E. A. Margulies, S. M. Dyar, R. J. Lindquist, Y. Wu, V. V. Roznyatovskiy, Y. Wu, R. M. Young, et al., *J. Phys. Chem. B* **2016**, *120*, 756–765.
[16] P. Irmler, F. S. Gogesch, C. B. Larsen, O. S. Wenger, R. F. Winter, *Dalton Trans.* **2019**, *48*, 1171–1174.
[17] P. Irmler, F. S. Gogesch, A. Mang, M. Bodensteiner, C. B. Larsen, O. S. Wenger, R. F. Winter, *Dalton Trans.* **2019**, *48*, 11690–11705.
[18] C. Bronner, O. S. Wenger, *Phys. Chem. Chem. Phys.* **2014**, *16*, 3617.
[19] J. Hankache, O. S. Wenger, *Phys. Chem. Chem. Phys.* **2012**, *14*, 2685.
[20] S. Mathew, H. Imahori, *J. Mater. Chem.* **2011**, *21*, 7166.
[21] A. C. Benniston, G. Copley, K. J. Elliott, R. W. Harrington, W. Clegg, *Eur. J. Org. Chem.* **2008**, *2008*, 2705–2713.
[22] A. C. Benniston, S. Clift, J. Hagon, H. Lemmetyinen, N. V. Tkachenko, W. Clegg, R. W. Harrington, *ChemPhysChem* **2012**, *13*, 3672–3681.
[23] F. A. Black, A. Jacquart, G. Toupalas, S. Alves, A. Proust, I. P. Clark, E. A. Gibson, G. Izzet, *Chem. Sci.* **2018**, *9*, 5578–5584.
[24] J. Bartelmess, A. J. Francis, K. A. El Roz, F. N. Castellano, W. W. Weare, R. D. Sommer, *Inorg. Chem.* **2014**, *53*, 4527–4534.
[25] V. Bandi, K. Ohkubo, S. Fukuzumi, F. D'Souza, *Chem. Commun.* **2013**, *49*, 2867.
[26] P. A. Liddell, G. Kodis, D. Kuciauskas, J. Andréasson, A. L. Moore, T. A. Moore, D. Gust, *Phys. Chem. Chem. Phys.* **2004**, *6*, 5509–5515.

[27] M. Hussain, A. M. El-Zohry, H. B. Gobeze, J. Zhao, F. D'Souza, O. F. Mohammed, *J. Phys. Chem. A* **2018**, *122*, 6081–6088.
[28] H. Imahori, M. E. El-Khouly, M. Fujitsuka, O. Ito, Y. Sakata, S. Fukuzumi, *J. Phys. Chem. A* **2001**, *105*, 325–332.
[29] D. Paul, J. A. Wytko, M. Koepf, J. Weiss, *Inorg. Chem.* **2002**, *41*, 3699–3704.
[30] M. Y. Lui, K. S. Lokare, E. Hemming, J. N. G. Stanley, A. Perosa, M. Selva, A. F. Masters, T. Maschmeyer, *RSC Adv.* **2016**, *6*, 58443–58451.
[31] L. Zhang, H. Chen, X. Zhao, Q. Zhai, D. Yin, Y. Sun, J. Li, *Appl. Catal. B* **2016**, *193*, 47–57.
[32] S. Ø. Scottwell, J. E. Barnsley, C. J. McAdam, K. C. Gordon, J. D. Crowley, *Chem. Commun.* **2017**, *53*, 7628–7631.
[33] K. Lee, J. C. Cho, J. DeHeck, J. Kim, *Chem. Commun.* **2006**, 1983–1985.
[34] K. Wariishi, S. I. Morishima, Y. Inagaki, *Org. Process Res. Dev.* **2003**, *7*, 98–100.
[35] A. Gouloumis, D. González-Rodríguez, P. Vázquez, T. Torres, S. Liu, L. Echegoyen, J. Ramey, G. L. Hug, D. M. Guldi, *J. Am. Chem. Soc.* **2006**, *128*, 12674–12684.
[36] F. Li, J. Cheng, X. Chai, S. Jin, X. Wu, G.-A. Yu, S. H. Liu, G. Z. Chen, *Organometallics* **2011**, *30*, 1830–1837.
[37] J. Jose, Y. Ueno, J. C. Castro, L. Li, K. Burgess, *Tetrahedron Lett.* **2009**, *50*, 6442–6445.
[38] M. Yu, J. K. H. Wong, C. Tang, P. Turner, M. H. Todd, P. J. Rutledge, *Beilstein J. Org. Chem.* **2015**, *11*, 37–41.
[39] M. H. Y. Cheng, H. Savoie, F. Bryden, R. W. Boyle, *Photochem. Photobiol. Sci.* **2017**, *16*, 1260–1267.
[40] J.-J. Cao, M.-S. Zhang, X.-Q. Li, D.-C. Yang, G. Xu, J.-Y. Liu, *Eur. J. Med. Chem.* **2020**, *193*, 112203.
[41] S. Cetindere, S. T. Clausing, M. Anjass, Y. Luo, S. Kupfer, B. Dietzek, C. Streb, *Chem. A Eur. J.* **2021**, *27*, 17181–17187.
[42] K. M. Ziems, S. Gräfe, S. Kupfer, *Catalysts* **2018**, *8*, 18–27.
[43] S. Ji, J. Ge, D. Escudero, Z. Wang, J. Zhao, D. Jacquemin, *J. Org. Chem.* **2015**, *80*, 5958–5963.
[44] S. Chibani, A. D. Laurent, B. Le Guennic, D. Jacquemin, *J. Chem. Theory Comput.* **2014**, *10*, 4574–4582.
[45] J. D. Spiegel, M. Kleinschmidt, A. Larbig, J. Tatchen, C. M. Marian, *J. Chem. Theory Comput.* **2015**, *11*, 4316–4327.
[46] M. R. Momeni, A. Brown, *J. Chem. Theory Comput.* **2015**, *11*, 2619–2632.
[47] L. Dura, M. Wächtler, S. Kupfer, J. Kübel, J. Ahrens, S. Höfler, M. Bröring, B. Dietzek, T. Beweries, *Inorganics* **2017**, *5*, 21.
[48] D. Costabel, A. Nabiyan, A. Chettri, F. Jacobi, M. Heiland, J. Guthmuller, S. Kupfer, M. Wächtler, B. Dietzek-Ivanšić, C. Streb, et al., *ACS Appl. Mater. Interfaces* **2023**, *15*, 20833–20842.
[49] Z.-H. Pan, G.-G. Luo, J.-W. Zhou, J.-X. Xia, K. Fang, R.-B. Wu, *Dalton Trans.* **2014**, *43*, 8499–8507.
[50] N. A. Romero, D. A. Nicewicz, *Chem. Rev.* **2016**, *116*, 10075–10166.
[51] V. Balzani, P. Ceroni, A. Juris, *Photochemistry and Photophysics Concepts, Research, Applications*, Wiley-VCH-Verl, Weinheim SE -, **2014**.
[52] E. Bassan, Y. Dai, D. Fazzi, A. Gualandi, P. G. Cozzi, F. Negri, P. Ceroni, *Photochem. Photobiol. Sci.* **2022**, *21*, 777–786.
[53] A. M. Brown, C. E. McCusker, J. K. McCusker, *Dalton Trans.* **2014**, *43*, 17635–17646.
[54] L. Zedler, A. K. Mengele, K. M. Ziems, Y. Zhang, M. Wächtler, S. Gräfe, T. Pascher, S. Rau, S. Kupfer, B. Dietzek, *Angew. Chem. Int. Ed.* **2019**, *58*, 13140–13148.
[55] J. T. Buck, A. M. Boudreau, A. DeCarmine, R. W. Wilson, J. Hampsey, T. Mani, *Chem* **2019**, *5*, 138–155.
[56] C. Müller, T. Pascher, A. Eriksson, P. Chabera, J. Uhlig, *J. Phys. Chem. A* **2022**, *126*, 4087–4099.
[57] J. Lefebvre, X. Sun, J. A. Calladine, M. W. George, E. A. Gibson, *Chem. Commun.* **2014**, *50*, 5258–5260.
[58] R. P. Sabatini, T. M. McCormick, T. Lazarides, K. C. Wilson, R. Eisenberg, D. W. McCamant, *J. Phys. Chem. Lett.* **2011**, *2*, 223–227.
[59] T. Yang, R. A. Arellano-Reyes, R. C. Curley, K. K. Jha, A. Chettri, T. E. Keyes, B. Dietzek-Ivanšić, *Chem. A Eur. J.* **2023**, *29*, DOI 10.1002/chem.202300224.
[60] T. Tran, J. Rabah, M.-H. Ha-Thi, E. Allard, S. Nizinski, G. Burdzinski, S. Aloïse, H. Fensterbank, K. Baczko, H. Nasrallah, et al., *J. Phys. Chem. B* **2020**, *124*, 9396–9410.

Manuscript received: October 4, 2023
Accepted manuscript online: February 27, 2024
Version of record online: March 14, 2024